Chemical composition, source, and process of urban aerosols during winter haze formation in Northeast China

Shi, Zongbo

DOI:
10.1016/j.envpol.2017.07.102

Document Version
Peer reviewed version

Citation for published version (Harvard):
Shi, Z 2017, 'Chemical composition, source, and process of urban aerosols during winter haze formation in Northeast China', Environmental Pollution, vol. 231, no. Part 1, pp. 357-366.
https://doi.org/10.1016/j.envpol.2017.07.102

Chemical composition, source, and process of urban aerosols during winter haze formation in Northeast China

Jian Zhang [a, b], Lei Liu [a], Yuanyuan Wang [a], Yong Ren [c], Xin Wang [c], Zongbo Shi [d], Daizhou Zhang [e], Huizheng Che [f], Hujia Zhao [g], Yanfei Liu [h], Hongya Niu [i], Jianmin Chen [a, j], Xiaoye Zhang [f], Zifa Wang [k], A.P. Lingaswamy [a], and Weijun Li [a, b *]

[a] *Environment Research Institute, Shandong University, Jinan, Shandong 250100, China*

[b] *Department of Atmospheric Sciences, School of Earth Sciences, Zhejiang University, Hangzhou, 320007, China*

[c] *Key Laboratory for Semi-Arid Climate Change of the Ministry of Education, College of Atmospheric Sciences, Lanzhou University, Lanzhou 730000, Gansu, China*

[d] *School of Geography, Earth and Environmental Sciences, University of Birmingham, Birmingham B15 2TT, UK*

[e] *Faculty of Environmental and Symbiotic Sciences, Prefectural University of Kumamoto, Kumamoto 862-8502, Japan*

[f] *Key Laboratory of Atmospheric Chemistry, Chinese Academy of Meteorological Sciences, Beijing 100081, China*

[g] *Institute of Atmospheric Environment, China Meteorological Administration, Shenyang 110016, China*

[h] *College of Environmental and Chemical Engineering, Heilongjiang University of Science and Technology, Harbin 150022, China*

[i] *Key Laboratory of Resource Exploration Research of Hebei Province, Hebei University of Engineering, Handan 056038, China*

[j] *Shanghai Key Laboratory of Atmospheric Particle Pollution and Prevention, Department of Environmental Science and Engineering, Fudan University, Shanghai 200433, China*

[k] *State Key Laboratory of Atmospheric Boundary Layer Physics and Atmospheric Chemistry, Institute of Atmospheric Physics, Chinese Academy of Sciences, Beijing 100029, China*

* *Corresponding Email: liweijun@zju.edu.cn (W. J. Li)*

Abstract The characteristics of aerosol particles have been poorly evaluated even though haze episodes frequently occur in winter in Northeast China. OC/EC analysis, ion chromatography, and transmission electron microscopy (TEM) were used to investigate the organic carbon (OC) and elemental carbon (EC), and soluble ions in $PM_{2.5}$ and the mixing state of individual particles during a severe wintertime haze episode in Northeast China. The organic matter (OM), NH_4^+, SO_4^{2-}, and NO_3^- concentrations in $PM_{2.5}$ were 89.5 μg/m^3, 24.2 μg/m^3, 28.1 μg/m^3, and 32.8 μg/m^3 on the haze days, respectively. TEM observations further showed that over 80% of the haze particles contained primary organic aerosols (POAs). Based on a comparison of the data obtained during the haze formation, we generate the following synthetic model of the process: (1) Stable synoptic meteorological conditions drove the haze formation. (2) The early stage of haze formation (light or moderate haze) was mainly caused by the enrichment of POAs from coal burning for household heating and cooking. (3) High levels of secondary organic aerosols (SOAs), sulfates, and nitrates formation via heterogeneous reactions together with POAs accumulation promoted to the evolution from light or moderate to severe haze. Compared to the severe haze episodes over the North China Plain, the $PM_{2.5}$ in Northeast China analyzed in the present study contained similar sulfate, higher SOA, and lower nitrate contents. Our results suggest that most of the POAs and secondary particles were likely related to emissions from coal-burning residential stoves in rural outskirts and small boilers in urban areas. The inefficient burning of coal for household heating and cooking should be monitored during wintertime in Northeast China.

1. Introduction

Massive amounts of primary and secondary anthropogenic particles are emitted or formed that can form a thick haze layer under stable synoptic meteorological conditions. Anthropogenic aerosol particles mainly consist of sulfates, nitrates, organics, black carbon (BC), fly ash, metal, and mineral dust (Bi et al., 2007; Denkenberger et al., 2007; Laskin et al., 2015; Li et al., 2016a; Moffet et al., 2008; Tian et al., 2015; Wang et al., 2009). The thick haze layer, varying from a few hundred meters to 2 km, blocks solar radiation from reaching the earth's surface and heats the planetary boundary layer through scattering and absorption by particulates and nitrogen dioxide gas (Ding et al., 2016; Ramanathan et al., 2001). High concentrations of aerosol particles transported from the ground can become cloud condensation nuclei (CCN) and modify the precipitation dynamics of clouds (Bennartz et al., 2011). Various anthropogenic particles and natural mineral dust can act as ice nuclei in clouds (Ren et al., 2017; Wang et al., 2015). Air pollution from coal-fired power plants and steel industries may fertilize ocean-dwelling plankton to better trap CO_2 and promote global cooling (Li et al., 2017). In addition, high concentrations of anthropogenic aerosol particles in urban air adversely affect human health, increasing the incidence of mortality, stroke, and cardiovascular and respiratory diseases (Lelieveld et al., 2015; Liu et al., 2017; Yang et al., 2013).

Rapid industrialization and urbanization in the last 30 years in China have caused severe air pollution, which is evident in the deterioration of both air quality (Zhang et al., 2015) and visibility (Che et al., 2007). Although the economy in Northeast China (Liaoning, Jilin, and Heilongjiang Provinces) has not increased as rapidly as in other areas, such as the North China Plain (NCP), Pearl River delta (PRD), and Yangtze River delta (YRD), in the past 10 years, its air quality deterioration is similar. Interestingly, the air quality in the heating season sharply contrasts that in the non-heating season in Northeast China. During the non-heating period, the average $PM_{2.5}$ concentration was approximately 30 $\mu g/m^3$. However, compared to the non-heating period, there was a higher number of haze days, and $PM_{2.5}$ concentration increased approximately 4-5 times during the heating period (lasting up to 5 months, from late-October to late-March of the next year). In recent years, the maximum concentration of hourly $PM_{2.5}$ greatly exceeded 1000 $\mu g/m^3$ during the wintertime heating period in Northeast China. For example, the hourly $PM_{2.5}$

concentration reached 1326 μg/m^3 in the city of Shenyang on 8 November 2015 and 1281 μg/m^3 in the city of Harbin on 4 November 2016. The above $PM_{2.5}$ values were derived from the Ministry of Environmental Protection of China (https://www.aqistudy.cn/). Because of these extremely elevated concentrations, a better understanding of the formation of severe regional haze in winter in Northeast China is necessary.

As air pollution has spread throughout China, scientists have primarily studied this pollution in the NCP, PRD, and YRD regions (Fu et al., 2008; He et al., 2011; Zhao et al., 2013). In the past 10 years, only a few studies have investigated aerosol particles in typically polluted locations of Northeast China, such as Longfeng Mountain (AOD_{440nm} was approximately stable at 0.9 on haze days) (Wang et al., 2010), Shenyang (average $PM_{2.5}$ concentration was approximately 130 μg/m^3 during wintertime) (Han et al., 2009), Tongyu (average BC concentration was approximately 2.52 μg/m^3 during the non-heating period) (Cheng et al., 2010), and Huludao (metal particles from traffic emissions) (Zheng et al., 2010). However, no study has investigated the formation mechanisms of regional haze in winter in Northeast China.

Because of the lack of studies of regional haze in Northeast China, it is difficult to draw comparisons with the haze pollution in the NCP, PRD, and YRD, which have been well documented in previous studies (Cheng et al., 2014; Deng et al., 2008; Tao et al., 2012). The Northeast China Plain is located between 40-48 °N and has a medium-latitude monsoon climate. Strong, prevailing winds from the northwest occur because of the influence of the cold high pressure systems over Siberia in winter. These strong cold winds push the haze layer out of the Northeast China Plain through the eastern canyon as shown in Figure 1. These haze particles can be further transported into the Korean Peninsula, the northern part of Japan, and the North Pacific Ocean (Dickerson et al., 2007; Jung et al., 2015; Lim et al., 2014). Therefore, studying the physicochemical characteristics of haze particles in winter in Northeast China could lead to greater understanding of their regional and global influences.

To assess the physical and chemical characteristics of aerosol particles and haze formation, a field experiment was carried out during a regional haze episode in Northeast China from 28 January to 7 February 2015. The mass concentrations, size distributions, and chemical compositions of aerosol particles were obtained. After the field work was completed, we determined the morphology and mixing state of individual aerosol particles by electron

microscopy for the first time.

2. Methods

2.1 Sampling site and sample collection

Northeast China consists of Liaoning, Jilin, and Heilongjiang Provinces and the eastern Inner Mongolia Autonomous Region. The Northeast China Plain is surrounded by the Lesser Khingan Mountains and the Changbai Mountains, and the Sanjiang Plain lies on the other side of these two mountain ranges, forming a canyon terrain (Figure 1). Jilin (43.83 °N, 126.55 °E) is a typical large city located in central Northeast China (Figure 1), and regional hazes in Northeast China are through Jilin under the influence between north and south transports. Therefore, Jilin is a representative sampling site to study the regional haze over Northeast China. There are ~4 million people living in Jilin City, and ~50% of the population is living in surrounding rural outskirts, based on the 2012 statistical yearbook of Jilin City. The sampling instruments were installed on a building roof located 15 m above the ground in the central urban Jilin surrounded by the residential areas and urban streets.

Ambient $PM_{2.5}$ samples were collected on 90 mm quartz filters for 23.5 h (8:00-7:30 (next day)) by a TH-150A sampler (Wuhan Tianhong Instrument) at a flow rate of 100 L/min. The filters were stored in a refrigerator at -2 °C until $PM_{2.5}$, organic carbon (OC), elemental carbon (EC), and water-soluble ion analyses.

Individual aerosol particles were collected on copper (Cu) grids coated with carbon (C) film by a DKL-2 sampler with a single-stage cascade impactor equipped with a 0.3 mm diameter jet nozzle at a flow of 1.0 L/min at 9:00, 15:00, and 20:00 local time every day. During the sampling period, we collected source samples from direct emissions of cooking and heating in rural outskirts. The collection efficiency of the impactor is 50% for particles with an aerodynamic diameter of 0.1 μm and a density of 2 g cm^{-3}. The Cu grids, stored in a dry, clean, and airtight container, were then analyzed by transmission electron microscopy (TEM) and atomic force microscopy (AFM).

Meteorological data including the relative humidity (RH), temperature, wind speed, and wind direction were measured and recorded every 5 min by an automated weather meter (Kestrel 5500,

USA).

2.2 $PM_{2.5}$, OC, EC, and water-soluble ion analyses

The quartz filters were weighed on a high-precision digital balance (Sartorius ME 5-F, reading precision of 0.001 mg) before and after sampling. The $PM_{2.5}$ mass concentrations were calculated according to the sampling duration, sampling flow rate, and weight difference of the quartz filters before and after sampling.

A rectangle of 1 × 1.5 cm^2 was removed from each quartz filter and placed in a quartz spoon. After the OC/EC analyzer (Sunset Lab) was preheated and calibrated, the spoon was placed into the quartz furnace for analysis. The mass concentrations of OC and EC were then calculated. Organic matter (OM) concentrations were obtained via multiplying OC concentrations by a factor of 1.4, which was reported by Guinot et al. (2007).

A quarter of each quartz filter was cut and placed into a clean plastic tube, and 10 ml of deionized water was added. After a 20 min ultrasonic bath, the solution was injected into a clean small plastic bottle via a 1 ml needle tube. To ensure the accuracy of the analytical results, this pretreatment had to be conducted twice for each quarter of every quartz filter. After calibration with standard solutions, the sample solutions were injected into the ion chromatography system (Dionex ICs-90) via a 1 ml syringe one after another for the determination of five cations (Na^+, K^+, NH_4^+, Ca^{2+}, and Mg^{2+}) and five anions (F^-, Cl^-, NO_2^-, NO_3^-, and SO_4^{2-}).

2.3 TEM analysis

The Cu grids were fixed on a sample rod that was inserted into the vacuum chamber of the TEM system (JEOL JEM-2100), which was combined with energy-dispersive X-ray spectrometry (EDS). A total of 1489 particles were analyzed by TEM/EDS at 200 kV. The morphology and mixing state of the aerosol particles were determined by TEM. EDS can detect elements with atomic weights corresponding to C and above. Cu was not quantified because the Cu grids would have led to interferences. The equivalent circle diameters (ECDs) of the particles were measured using iTEM software. To reduce the damage to particles under the electron beam, the EDS collection duration was limited to within 15 s (Li et al., 2011). Particles in 3-5 grids of each sample were analyzed to ensure their universality and representativeness.

2.4 AFM analysis

As an analytical instrument for studying the surface structure of solid materials, AFM

(Dimension Icon) can determine the three-dimensional morphology of particles in tapping mode via a probe that taps the particles. The force between the probe and sample, the scanning rate, and the scanning range were 1-1.5 nN, 0.5-0.8 Hz, and 10 μm, respectively, with a resolution of 512 pixels per length. The bearing areas (A) and bearing volumes (V) of the particles were directly obtained from the Nanoscope Analysis software. Their ECDs and equivalent volume diameters (EVDs) were calculated according to the following formulas (Chi et al., 2015):

$$ECD=\sqrt{\frac{4A}{\pi}} \quad (1)$$

$$EVD=\sqrt[3]{\frac{6V}{\pi}} \quad (2)$$

where π is 3.14.

The regressions of the ECDs versus the EVDs (ECD vs EVD) were obtained and are shown in Figure S2. The EVDs of all the analyzed particles could be calculated using the equations.

3. Results

3.1 Meteorological characteristics and pollutant concentrations

A typical regional haze episode occurred over Northeast China on 1-4 February 2015, based on reports from the Chinese Meteorological Administration (CMA), and daily $PM_{2.5}$ concentrations exceeded 150 μg/m^3 (Figure 2). The haze episode ended on 5 February due to a strong west wind (Figure S3). During 28-31 January and 5-7 February, most of the hourly $PM_{2.5}$ mass concentrations were lower than 75 μg/m^3 and the visibility was higher than or close to 10 km, although $PM_{2.5}$ in a few hours around 7:00-9:00 and 16:00-18:00 had peaks higher than 75 μg/m^3, based on the Ministry of Environmental Protection of China. Moreover, the CMA had no any report about occurrence of the regional haze during 28-31 January and 5-7 February in Northeast China. In this study, they were designated non-haze days. The variations in temperature and RH showed an opposite trend every day during the sampling period (Figures S3b-c). The temperature generally increased, with the average value ranging from -17.7 to 5.1 °C (Figure S3b), and the RH increased from 51% during the day to 74% at night during the haze period (Figure S3c).

Three trace gases (i.e., CO, SO_2, and NO_2) were two times higher on the haze days than on

193 the non-haze days, and their maximum values reached 2.93 ppm, 72 ppb, and 65 ppb on 3
194 February, respectively (Figure S4).

195 Figure 2 shows that the $PM_{2.5}$ with an average concentration of 97 μg/m^3 on the non-haze
196 days and 245 μg/m^3 on the haze days. During 3-4 February, the average $PM_{2.5}$ concentration was
197 289 μg/m^3 (Figure 2), which exceeds 250 μg/m^3, the threshold for severe haze days of the Chinese
198 National Ambient Air Quality Standards. According to these standards, 1-2 February, with an
199 average $PM_{2.5}$ concentration of 201 μg/m^3 (Figure 2), were moderate haze days. The highest daily
200 $PM_{2.5}$ concentration reached 310 μg/m^3 on 3 February (Figure 2). The average concentrations of
201 OM, NH_4^+, SO_4^{2-}, and NO_3^- were 28.6 μg/m^3, 10.5 μg/m^3, 10.6 μg/m^3, and 22.9 μg/m^3 on the
202 non-haze days, accounting for 30%, 11%, 11%, and 24% of the daily $PM_{2.5}$ concentration,
203 respectively (Figure 2). On the haze days, these four species were 89.5 μg/m^3, 24.2 μg/m^3, 28.1
204 μg/m^3, and 32.8 μg/m^3, accounting for 37%, 10%, 11%, and 13% of the $PM_{2.5}$ concentration of
205 245 μg/m^3, respectively (Figure 2). The highest concentrations of OM, NH_4^+, SO_4^{2-}, and NO_3^-
206 were 112.4 μg/m^3, 33.8 μg/m^3, 44.0 μg/m^3, and 39.4 μg/m^3 on 3 February (Figure 2). The
207 concentrations of OM, EC, NH_4^+, SO_4^{2-}, NO_3^-, and Cl^- in $PM_{2.5}$ increased approximately 2.1, 1.0,
208 1.3, 1.7, 0.4, and 2.1 times from the non-haze to the haze days. Therefore, during the sampling
209 period, the concentrations of OM were the highest in $PM_{2.5}$ in terms of the individual species, and,
210 in total, the OM and secondary inorganic ions (NH_4^+, SO_4^{2-}, and NO_3^-) were dominant in $PM_{2.5}$
211 (Figure 2). The difference between the sum of chemical species and $PM_{2.5}$ concentration should be
212 attributed to contributions of minerals, fly ash, and heavy metals to $PM_{2.5}$, based on the results of
213 TEM observations.

214 **3.2 Classification and mixing state of individual particles**

215 Based on the elemental composition and morphology of individual particles, we classified
216 four major aerosol components: organics, soot, S-rich, and fly ash/metal (Figures 3a-f).

217 Organic particles, as the most common particle in the samples, were stable under the strong
218 electron beam of TEM and were composed of C, O, and Si, as well as minor amounts of N, S, and
219 Cl (Figures 3a-c). Based on their different morphologies, the organic particles were further divided
220 into dome-like (Figure 3a), irregular (Figure 3b), spherical (Figure 3c), and organic-coated
221 particles. Interestingly, the former three types were dominant in the air influenced by the direct
222 emissions from coal burning for cooking and heating in a residential stove (Figure S5). As a result,

they were defined as primary organic aerosols (POAs). Organic-coated particles, which consist of organic coatings on mostly other types of particles, were identified as secondary organic aerosols (SOAs) (Adachi and Buseck, 2008; Li et al., 2016b). POAs with an average O/C ratio of 0.21 was much lower than 0.44 of SOAs (Figure S6). In this study, most of the POAs and SOAs were internally mixed with soot, S-rich particles, or fly ash/metal particles (Figures 4a-f).

Soot particles present a chain-like morphology consisting of an aggregate of carbonaceous spheres with diameters from 10 to 150 nm (Figures 3d and 4d). Soot particles were internally mixed with the organic particles and mainly contained C and minor amounts of O (Figure 3d).

The S-rich particles were sensitive to the strong electron beam and were mainly composed of S, O, and N, as well as minor amounts of K and Na in this study (Figure 3e). S-rich particles generally represent secondary inorganic aerosols containing NH_4NO_3 and $(NH_4)_2SO_4$ (Li et al., 2016b). The S-rich particles were internally mixed with organic particles (Figures 4a-f), soot (Figure 4d), fly ash particles (Figure 4e), and metal particles (Figure 4f).

The fly ash/metal particles generally were smaller than 200 nm; spherical (Figures 3f and 4e-f); and mainly contained O, Si, and Al, as well as minor amounts of metallic elements such as Fe, Mn, Pb, and Zn (Figure 3f). These particles have been considered tracers of coal combustion in industrial activities and power plants (Li and Shao, 2009).

In this study, based on the mixing state of the above aerosol components within the individual particles, we further classified the particles into five major types: organic-rich (Figures 3a-c), organic-S (Figures 4a-c), organic-soot (Figure 4d), S-fly ash (Figure 4e), and S-metal (Figure 4f).

3.3 Relative abundance of individual particles

Among all the analyzed aerosol particles, TEM observations clearly showed that more than 80% of individual particles contained POAs such as dome-like organic, irregular organic, and spherical organic particles (indicated by the red frame in Figure 5). On the non-haze days, the relative abundance of organic-rich particles (37%) was nearly same as that of organic-S particles (39%) but higher than that of organic-soot particles (22%) (Figure 5). S-fly ash and S-metal particles both occupied only 1% of all the analyzed particles on the non-haze days (Figure 5). On the haze days, the relative abundance of organic-S, S-fly ash, and S-metal particles increased in the samples. Figure 5 shows that the maximum proportions of organic-S, S-fly ash, and S-metal particles were 66%, 8%, and 4% on 3 February, respectively.

3.4 Size distribution of individual particles

Figure 6 shows the size distributions of individual particles on the non-haze and haze days. On the non-haze days, the size distribution of individual particles shows a peak at 249 nm (Figure 6); on the haze days, the peak is at 386 nm (Figure 6). This difference can be attributed to the formation of S-rich particles and SOAs on preexisting particles during the haze period which can increase the particle size (see section 4.2). Notably, the slope of ECD vs EVD on the haze days (0.3798) is much lower than that on the non-haze days (0.6238) (Figure S2), showing that individual haze particles spread out on the substrate (Figure S2b) and retained their liquid phase in the higher RH air (52-89%) (Figure S3c).

4. Discussion

4.1 Sources of organic particles

The OM mass fractions in $PM_{2.5}$ increased from 30% on the non-haze days to 37% on the haze days (Figure 2), and TEM observations revealed that the relative abundance of organic-containing particles exceeded 80% on the haze days (Figure 5). These results are different from the findings of some previous studies during summer haze period caused by heavy industries, vehicle exhaust, and coal-fired power plants (Li et al., 2016b; Yuan et al., 2015), which indicated S-rich particles were most abundant, although a few S-rich particles contained POA inclusions (i.e., dome-like organic, irregular organic, and spherical organic particles). The comparison suggests that abundant POAs should not be directly emitted from heavy industries, vehicle exhaust, and coal-fired power plants over Northeast China.

Li et al. (2012) found a large number of spherical POA particles in a coal-burning area over the China Loess Plateau during the winter heating period. POA particles were the most abundant in winter at the rural site in Northeast China (Xu et al., 2017). Moreover, some studies noted that the concentrations of organic particles from emissions of industrial boiler and coal-fired power plants were far lower than those from coal and biomass burning in residential stoves (Liu et al., 2016; Zhang et al., 2008). Coal and biomass burning both directly emit high levels of volatile organic compounds and semi-volatile organic compounds in the smog (Huang et al., 2014; Schnelle-Kreis et al., 2007; Xu et al., 2015), which can form SOAs. Although biomass or wood

burning can also emit large amounts of organic particles (Florou et al., 2017; Paraskevopoulou et al., 2015), Figure 2 shows that Cl^- concentrations were much higher than the K^+ content in $PM_{2.5}$, which is the opposite of the K/Cl ratio emitted by biomass burning (Pósfai et al., 2003). Here we excluded Cl^- was from sea salts based on TEM observations. TEM/EDS showed that Cl was detected in the POAs (Figure 3c), which is consistent with the chemical composition of spherical organics emitted by coal burning (Li et al., 2012). We did observe high levels of POAs (i.e., dome-like organic, irregular organic, and spherical organic particles) from the direct emissions of coal burning in residential stoves (Figure S5). Therefore, we can infer that most of the organic particles were likely related to coal burning emission, although we could not exclude a certain contribution from the emissions of biomass burning (Figure S7). Moreover, under the stable synoptic conditions (e.g., wind speed lower than 1.3 m/s) (Figure S3), regional transports of air pollutants played a minor role. After sunrise during the daytime, vertical transports of air pollutants possibly occupied a certain proportion in the regional contribution of fine particles. We noticed that consistent and strong household heating via coal combustion is necessary in Northeast China due to the rather low temperatures that can reach ~-20 ℃ in winter. Some small boilers were used in the urban areas of Jilin, although ~40% of the population were living in the rural outskirts and were using residential stoves for household heating and cooking, based on the demographics of Northeast China (Jilin, Liaoning, and Heilongjiang Provinces) listed in the statistical yearbooks of 2015. In this study, we concluded that these organic particles were mainly related to coal-burning residential stoves in the rural outskirts and small boilers in the urban areas.

4.2 Formation mechanisms of the regional haze

The mass concentrations of OM and secondary inorganic ions (NH_4^+, SO_4^{2-}, and NO_3^-) in $PM_{2.5}$ significantly increased from the non-haze days to the haze days (Figure 2). SO_4^{2-}/EC, NO_3^-/EC, and OC/EC can be indicative of pollutant accumulation due to changes in the atmospheric boundary layer as well as of the secondary formation of species such as sulfates, nitrates, and SOAs during haze formation (Zheng et al., 2015). The sulfur oxidation ratio (SOR) and nitrogen oxidation ratio (NOR) values of 0.20 and 0.24 on the haze days (Figure S8) are lower than the reported values of 0.29 and 0.51 (Zhao et al., 2013) and 0.34 and 0.28 (Zheng et al., 2015) on haze days in winter in the NCP, respectively. However, OC/EC increased on the haze days and with value of 6.55 (Figure 7b) is much higher than the ratios of 4.53, 4.40, 4.09, and 4.34 reported

in different cities in the NCP (Zhao et al., 2013). These above comparisons indicate that organic aerosols made a larger contribution to haze formation than sulfates and nitrates in winter in Northeast China, which is consistent with the TEM observations indicating that abundant SOAs and POAs occurred together on the haze days compared with lesser amounts on the non-haze days (Figures 8a-b).

During the early stage of the haze episode (1-2 February (moderate haze in this study)), the $PM_{2.5}$ level increased, OC/EC consistently increased from 4.08 to 6.01, SO_4^{2-}/EC remained stable at 1.92, and NO_3^-/EC decreased from 3.99 to 2.64 compared to the non-haze days during 28-31 January (Figures 2 and 7a-b). Moreover, the increasing trends of $PM_{2.5}$/EC and OC/EC were similar during the moderate haze days (Figure 7b). These results are consistent with the TEM observations, which showed that high levels of POAs were dominant in the samples during the moderate haze days (Figure 5). In addition, the lower temperatures and higher RH during the haze period likely drove substantial amounts of semi-volatile organic compounds from coal burning to the particulate phase (i.e., SOAs) (Lim and Turpin, 2002). Therefore, the increase in the mixture of POAs and SOAs promoted the moderate haze formation during 1-2 February.

During the severe haze period (3-4 February), the SOR, RH, and $PM_{2.5}$ concentrations all increased compared to those on the moderate haze days (Figures 2, S3c, and S8). In addition, the AFM image illustrates that the haze particles were wet aerosols in the ambient air (Figure S2b). TEM observations demonstrated that the hygroscopic SOAs on particle surfaces could provide an aqueous media that can promote the conversion of SO_2 to sulfates through heterogeneous reactions during severe haze periods (Wang et al., 2016). This phenomenon has widely occurred in humid air during severe haze formation in the NCP (Cheng et al., 2016). Our results show that SO_4^{2-}/EC, NO_3^-/EC, OC/EC, and $PM_{2.5}$/EC increased during the severe haze period (Figures 7a-b). Compared to the moderate haze days, $PM_{2.5}$/EC increased 64% during the severe haze period, which is significantly higher than the increase in OC/EC of 18% (Figure 7b). As a result, the considerable formation of sulfates, nitrates, and SOAs and the accumulation of POAs together promoted the evolution of moderate haze to severe haze.

Compared to the non-haze days, SO_4^{2-}/EC increased 107% during the severe haze period in winter in Northeast China (Figure 7a), which is effectively equal to the increase of 110% determined by Zheng et al. (2015) in winter in the NCP. NO_3^-/EC only increased 9% (Figure 7a),

which is much lower than the 77% increase reported by Zheng et al. (2015) in the NCP. Moreover, OC/EC increased 74% (Figure 7b), which is higher than the value of ~45% reported by Zhao et al. (2013) in the NCP. These comparisons suggest many differences between the severe haze particles of the NCP and Northeast China. Therefore, the increase in organics and sulfates instead of nitrates promoted the severe haze formation in winter in Northeast China compared to the severe haze episodes in the NCP.

5. Conclusions and implications

An aerosol experiment was carried out over the city of Jilin in central Northeast China from 28 January to 7 February 2015. A regional haze episode occurred during 1-4 February. On the haze days, the levels of three anthropogenic gases (i.e., CO, SO_2, and NO_2) were twice as high as those on the non-haze days. The $PM_{2.5}$ concentrations were 2.5 times higher on the haze days than on the non-haze days, and the highest daily $PM_{2.5}$ concentration reached 310 μg/m^3. Furthermore, OM and secondary inorganic ions (NH_4^+, SO_4^{2-}, and NO_3^-) were the dominant species in $PM_{2.5}$, and their concentrations increased 2.1, 1.3, 1.7, and 0.4 times on the haze days compared to the non-haze days, respectively. The fold changes of the secondary inorganic ion concentrations in this study were lower than the fold changes of 4.3-9.1 reported by Zhao et al. (2013) in winter in the NCP.

We divided the aerosol particles into five types: organic-rich, organic-S, organic-soot, S-fly ash, and S-metal, based on the mixing state, composition, and morphology of individual particles. We found that the relative abundance of organic-related particles exceeded 80% during the haze days, which is higher than the level of 70% recorded during moderate haze episodes in winter in the NCP (Chen et al., 2017). Our study revealed that most of the organic particles were related to the emissions of coal-burning residential stoves in the rural outskirts and small boilers in the urban areas. Moreover, biomass burning may be a second source.

To systematically consider the changes of the different aerosols in $PM_{2.5}$ and individual particles based on the TEM observations on non-haze and haze days, we proposed the following conceptual model (Figure 9) that reflected the haze formation mechanisms in winter in Northeast China. With the advent of stable synoptic conditions (e.g., wind speeds decrease and RH increase),

the enrichment of POAs from coal burning for household heating and cooking likely caused the early-stage formation of haze (light or moderate haze). Meanwhile, solar radiation was reduced by the haze layer, and photochemical activity was weakened. During the severe haze period, heterogeneous reactions became the major formation pathway of secondary aerosols under high RH. Our results show that the increase in sulfates and organics instead of nitrates promoted the evolution of moderate to severe haze in Northeast China compared to the severe haze formation over the NCP. In summary, the high-intensity emissions from inefficient coal burning for heating and cooking in winter in the rural outskirts and urban areas can cause the regional haze in Northeast China under the right meteorological conditions.

Acknowledgments

We thank Peter Hyde for his editorial comments. This work was funded by the National Natural Science Foundation of China (41575116, 41622504, and 41522505) and Shandong Provincial Science Fund for Distinguished Young Scholars (JQ201413). All images and the related additional data are available from WJL (email: liweijun.atmos@gmail.com).

References

Adachi, K., Buseck, P., 2008. Internally mixed soot, sulfates, and organic matter in aerosol particles from Mexico City. Atmos. Chem. Phys. 8, 6469-6481.

Bennartz, R., Fan, J., Rausch, J., Leung, L.R., Heidinger, A.K., 2011. Pollution from China increases cloud droplet number, suppresses rain over the East China Sea. Geophys. Res. Lett. 38, L09704.

Bi, X., Thomas, G.O., Jones, K.C., Qu, W., Sheng, G., Martin, F.L., Fu, J., 2007. Exposure of electronics dismantling workers to polybrominated diphenyl ethers, polychlorinated biphenyls, and organochlorine pesticides in South China. Environ. Sci. Technol. 41, 5647-5653.

Che, H., Zhang, X., Li, Y., Zhou, Z., Qu, J.J., 2007. Horizontal visibility trends in China 1981–2005. Geophys. Res. Lett. 34, L24706.

Chen, S., Xu, L., Zhang, Y., Chen, B., Wang, X., Zhang, X., Zheng, M., Chen, J., Wang, W., Sun, Y., Fu, P., Wang, Z., Li, W., 2017. Direct observations of organic aerosols in common wintertime hazes in North China: insights into direct emissions from Chinese residential stoves. Atmos. Chem. Phys. 17, 1259-1270.

Cheng, T., Han, Z., Zhang, R., Du, H., Jia, X., Wang, J., Yao, J., 2010. Black carbon in a continental semi-arid area of Northeast China and its possible sources of fire emission. J. Geophys. Res. 115, D23204.

Cheng, Y., Zheng, G., Wei, C., Mu, Q., Zheng, B., Wang, Z., Gao, M., Zhang, Q., He, K., Carmichael, G., 2016. Reactive nitrogen chemistry in aerosol water as a source of sulfate during haze events in China. Sci. Adv. 2, e1601530.

Cheng, Z., Wang, S., Fu, X., Watson, J.G., Jiang, J., Fu, Q., Chen, C., Xu, B., Yu, J., Chow, J.C., Hao, J., 2014. Impact of biomass burning on haze pollution in the Yangtze River delta, China: a case study in summer 2011. Atmos. Chem. Phys. 14, 4573-4585.

Chi, J.W., Li, W.J., Zhang, D.Z., Zhang, J.C., Lin, Y.T., Shen, X.J., Sun, J.Y., Chen, J.M., Zhang, X.Y., Zhang, Y.M., Wang, W.X., 2015. Sea salt aerosols as a reactive surface for inorganic and organic acidic gases in the Arctic troposphere. Atmos. Chem. Phys. 15, 11341-11353.

Deng, X., Tie, X., Wu, D., Zhou, X., Bi, X., Tan, H., Li, F., Jiang, C., 2008. Long-term trend of visibility and its characterizations in the Pearl River Delta (PRD) region, China. Atmos. Environ. 42, 1424-1435.

Denkenberger, K.A., Moffet, R.C., Holecek, J.C., Rebotier, T.P., Prather, K.A., 2007. Real-time, single-particle measurements of oligomers in aged ambient aerosol particles. Environ. Sci. Technol. 41, 5439-5446.

Dickerson, R.R., Li, C., Li, Z., Marufu, L.T., Stehr, J.W., McClure, B., Krotkov, N., Chen, H., Wang, P., Xia, X., Ban, X., Gong, F., Yuan, J., Yang, J., 2007. Aircraft observations of dust and pollutants over northeast China: Insight into the meteorological mechanisms of transport. J. Geophys. Res. 112, D24S90.

Ding, A.J., Huang, X., Nie, W., Sun, J.N., Kerminen, V.M., Petäjä, T., Su, H., Cheng, Y.F., Yang, X.Q., Wang, M.H., Chi, X.G., Wang, J.P., Virkkula, A., Guo, W.D., Yuan, J., Wang, S.Y., Zhang, R.J., Wu, Y.F., Song, Y., Zhu, T., Zilitinkevich, S., Kulmala, M., Fu, C.B., 2016. Enhanced haze pollution by black carbon in megacities in China. Geophys. Res. Lett. 43, 2873-2879.

Florou, K., Papanastasiou, D.K., Pikridas, M., Kaltsonoudis, C., Louvaris, E., Gkatzelis, G.I., Patoulias, D., Mihalopoulos, N., Pandis, S.N., 2017. The contribution of wood burning and other pollution sources to wintertime organic aerosol levels in two Greek cities. Atmos. Chem. Phys. 17, 3145-3163.

Fu, Q., Zhuang, G., Wang, J., Xu, C., Huang, K., Li, J., Hou, B., Lu, T., Streets, D.G., 2008. Mechanism of formation of the heaviest pollution episode ever recorded in the Yangtze River Delta, China. Atmos. Environ. 42, 2023-2036.

Guinot, B., Cachier, H., Oikonomou, K., 2007. Geochemical perspectives from a new aerosol chemical mass closure. Atmos. Chem. Phys. 7, 1657-1670.

Han, B., Kong, S., Bai, Z., Du, G., Bi, T., Li, X., Shi, G., Hu, Y., 2009. Characterization of Elemental Species in PM2.5 Samples Collected in Four Cities of Northeast China. Water Air Soil Poll. 209, 15-28.

He, L.-Y., Huang, X.-F., Xue, L., Hu, M., Lin, Y., Zheng, J., Zhang, R., Zhang, Y.-H., 2011. Submicron aerosol analysis and organic source apportionment in an urban atmosphere in Pearl River Delta of China using high-resolution aerosol mass spectrometry. J. Geophys. Res. 116, D12304.

Huang, R.J., Zhang, Y., Bozzetti, C., Ho, K.F., Cao, J.J., Han, Y., Daellenbach, K.R., Slowik, J.G., Platt, S.M., Canonaco, F., Zotter, P., Wolf, R., Pieber, S.M., Bruns, E.A., Crippa, M., Ciarelli, G., Piazzalunga, A., Schwikowski, M., Abbaszade, G., Schnelle-Kreis, J., Zimmermann, R., An, Z.,

Szidat, S., Baltensperger, U., El Haddad, I., Prevot, A.S., 2014. High secondary aerosol contribution to particulate pollution during haze events in China. Nature 514, 218-222.

Jung, J., Lee, K., Cayetano, M.G., Batmunkh, T., Kim, Y.J., 2015. Optical and hygroscopic properties of long-range transported haze plumes observed at Deokjeok Island off the west coast of the Korean Peninsula under the Asian continental outflows. J. Geophys. Res.-Atmos. 120, 8861-8877.

Laskin, A., Laskin, J., Nizkorodov, S.A., 2015. Chemistry of atmospheric brown carbon. Chem. Rev. 115, 4335-4382.

Lelieveld, J., Evans, J.S., Fnais, M., Giannadaki, D., Pozzer, A., 2015. The contribution of outdoor air pollution sources to premature mortality on a global scale. Nature 525, 367-371.

Li, W., Shao, L., 2009. Transmission electron microscopy study of aerosol particles from the brown hazes in northern China. J. Geophys. Res. 114, D09302.

Li, W., Shao, L., Zhang, D., Ro, C.-U., Hu, M., Bi, X., Geng, H., Matsuki, A., Niu, H., Chen, J., 2016a. A review of single aerosol particle studies in the atmosphere of East Asia: morphology, mixing state, source, and heterogeneous reactions. J. Clean. Prod. 112, 1330-1349.

Li, W., Shi, Z., Zhang, D., Zhang, X., Li, P., Feng, Q., Yuan, Q., Wang, W., 2012. Haze particles over a coal-burning region in the China Loess Plateau in winter: Three flight missions in December 2010. J. Geophys. Res.-Atmos. 117, D12306.

Li, W., Sun, J., Xu, L., Shi, Z., Riemer, N., Sun, Y., Fu, P., Zhang, J., Lin, Y., Wang, X., Shao, L., Chen, J., Zhang, X., Wang, Z., Wang, W., 2016b. A conceptual framework for mixing structures in individual aerosol particles. J. Geophys. Res.-Atmos. 121, 13784-13798.

Li, W., Xu, L., Liu, X., Zhang, J., Lin, Y., Yao, X., Gao, H., Zhang, D., Chen, J., Wang, W., 2017. Air pollution–aerosol interactions produce more bioavailable iron for ocean ecosystems. Sci. Adv. 3, e1601749.

Li, W., Zhou, S., Wang, X., Xu, Z., Yuan, C., Yu, Y., Zhang, Q., Wang, W., 2011. Integrated evaluation of aerosols from regional brown hazes over northern China in winter: Concentrations, sources, transformation, and mixing states. J. Geophys. Res. 116, D09301.

Lim, H.-J., Turpin, B.J., 2002. Origins of primary and secondary organic aerosol in Atlanta: Results of time-resolved measurements during the Atlanta supersite experiment. Environ. Sci. Technol. 36, 4489-4496.

476 Lim, S., Lee, M., Kim, S.W., Yoon, S.C., Lee, G., Lee, Y.J., 2014. Absorption and scattering
477 properties of organic carbon versus sulfate dominant aerosols at Gosan climate observatory in
478 Northeast Asia. Atmos. Chem. Phys. 14, 7781-7793.
479 Liu, J., Mauzerall, D.L., Chen, Q., Zhang, Q., Song, Y., Peng, W., Klimont, Z., Qiu, X., Zhang, S.,
480 Hu, M., Lin, W., Smith, K.R., Zhu, T., 2016. Air pollutant emissions from Chinese households: A
481 major and underappreciated ambient pollution source. P. Natl. Acad. Sci. USA 113, 7756-7761.
482 Liu, M., Huang, Y., Ma, Z., Jin, Z., Liu, X., Wang, H., Liu, Y., Wang, J., Jantunen, M., Bi, J.,
483 Kinney, P.L., 2017. Spatial and temporal trends in the mortality burden of air pollution in China:
484 2004-2012. Environ. Int. 98, 75-81.
485 Moffet, R., Foy, B.d., Molina, L.a., Molina, M., Prather, K., 2008. Measurement of ambient
486 aerosols in northern Mexico City by single particle mass spectrometry. Atmos. Chem. Phys. 8,
487 4499-4516.
488 Pósfai, M., Simonics, R., Li, J., Hobbs, P.V., Buseck, P.R., 2003. Individual aerosol particles from
489 biomass burning in southern Africa: 1. Compositions and size distributions of carbonaceous
490 particles. J. Geophys. Res.-Atmos. 108, D13.
491 Paraskevopoulou, D., Liakakou, E., Gerasopoulos, E., Mihalopoulos, N., 2015. Sources of
492 atmospheric aerosol from long-term measurements (5 years) of chemical composition in Athens,
493 Greece. Sci. Total Environ. 527-528, 165-178.
494 Ramanathan, V., Crutzen, P.J., Lelieveld, J., Mitra, A.P., Althausen, D., Anderson, J., Andreae,
495 M.O., Cantrell, W., Cass, G.R., Chung, C.E., Clarke, A.D., Coakley, J.A., Collins, W.D., Conant,
496 W.C., Dulac, F., Heintzenberg, J., Heymsfield, A.J., Holben, B., Howell, S., Hudson, J., Jayaraman,
497 A., Kiehl, J.T., Krishnamurti, T.N., Lubin, D., McFarquhar, G., Novakov, T., Ogren, J.A.,
498 Podgorny, I.A., Prather, K., Priestley, K., Prospero, J.M., Quinn, P.K., Rajeev, K., Rasch, P.,
499 Rupert, S., Sadourny, R., Satheesh, S.K., Shaw, G.E., Sheridan, P., Valero, F.P.J., 2001. Indian
500 Ocean Experiment: An integrated analysis of the climate forcing and effects of the great
501 Indo-Asian haze. J. Geophys. Res.-Atmos. 106, 28371-28398.
502 Ren, Y., Zhang, X., Wei, H., Xu, L., Zhang, J., Sun, J., Wang, X., Li, W., 2017. Comparisons of
503 methods to obtain insoluble particles in snow for transmission electron microscopy. Atmos.
504 Environ. 153, 61-69.
505 Schnelle-Kreis, J., Sklorz, M., Orasche, J., Stölzel, M., Peters, A., Zimmermann, R., 2007. Semi

volatile organic compounds in ambient PM2. 5. Seasonal trends and daily resolved source contributions. Environ. Sci. Technol. 41, 3821-3828.

Tao, M., Chen, L., Su, L., Tao, J., 2012. Satellite observation of regional haze pollution over the North China Plain. J. Geophys. Res.-Atmos. 117, D12203.

Tian, H.Z., Zhu, C.Y., Gao, J.J., Cheng, K., Hao, J.M., Wang, K., Hua, S.B., Wang, Y., Zhou, J.R., 2015. Quantitative assessment of atmospheric emissions of toxic heavy metals from anthropogenic sources in China: historical trend, spatial distribution, uncertainties, and control policies. Atmos. Chem. Phys. 15, 10127-10147.

Wang, G., Zhang, R., Gomez, M.E., Yang, L., Levy Zamora, M., Hu, M., Lin, Y., Peng, J., Guo, S., Meng, J., Li, J., Cheng, C., Hu, T., Ren, Y., Wang, Y., Gao, J., Cao, J., An, Z., Zhou, W., Li, G., Wang, J., Tian, P., Marrero-Ortiz, W., Secrest, J., Du, Z., Zheng, J., Shang, D., Zeng, L., Shao, M., Wang, W., Huang, Y., Wang, Y., Zhu, Y., Li, Y., Hu, J., Pan, B., Cai, L., Cheng, Y., Ji, Y., Zhang, F., Rosenfeld, D., Liss, P.S., Duce, R.A., Kolb, C.E., Molina, M.J., 2016. Persistent sulfate formation from London Fog to Chinese haze. P. Natl. Acad. Sci. USA 113, 13630-13635.

Wang, P., Che, H., Zhang, X., Song, Q., Wang, Y., Zhang, Z., Dai, X., Yu, D., 2010. Aerosol optical properties of regional background atmosphere in Northeast China. Atmos. Environ. 44, 4404-4412.

Wang, X., Pu, W., Zhang, X., Ren, Y., Huang, J., 2015. Water-soluble ions and trace elements in surface snow and their potential source regions across northeastern China. Atmos. Environ. 114, 57-65.

Wang, X., Zhang, Y., Chen, H., Yang, X., Chen, J., Geng, F., 2009. Particulate nitrate formation in a highly polluted urban area: a case study by single-particle mass spectrometry in Shanghai. Environ. Sci. Technol. 43, 3061-3066.

Xu, L., Liu, L., Zhang, J., Zhang, Y., Ren, Y., Wang, X., Li, W., 2017. Morphology, Composition, and Mixing State of Individual Aerosol Particles in Northeast China during Wintertime. Atmosphere 8, 47-57.

Xu, W.Q., Sun, Y.L., Chen, C., Du, W., Han, T.T., Wang, Q.Q., Fu, P.Q., Wang, Z.F., Zhao, X.J., Zhou, L.B., Ji, D.S., Wang, P.C., Worsnop, D.R., 2015. Aerosol composition, oxidation properties, and sources in Beijing: results from the 2014 Asia-Pacific Economic Cooperation summit study. Atmos. Chem. Phys. 15, 13681-13698.

Yang, G., Wang, Y., Zeng, Y., Gao, G.F., Liang, X., Zhou, M., Wan, X., Yu, S., Jiang, Y., Naghavi, M., Vos, T., Wang, H., Lopez, A.D., Murray, C.J.L., 2013. Rapid health transition in China, 1990–2010: findings from the Global Burden of Disease Study 2010. Lancet 381, 1987-2015.

Yuan, Q., Li, W., Zhou, S., Yang, L., Chi, J., Sui, X., Wang, W., 2015. Integrated evaluation of aerosols during haze-fog episodes at one regional background site in North China Plain. Atmos. Res. 156, 102-110.

Zhang, X.Y., Wang, J.Z., Wang, Y.Q., Liu, H.L., Sun, J.Y., Zhang, Y.M., 2015. Changes in chemical components of aerosol particles in different haze regions in China from 2006 to 2013 and contribution of meteorological factors. Atmos. Chem. Phys. 15, 12935-12952.

Zhang, Y., Schauer, J.J., Zhang, Y., Zeng, L., Wei, Y., Liu, Y., Shao, M., 2008. Characteristics of particulate carbon emissions from real-world Chinese coal combustion. Environ. Sci. Technol. 42, 5068-5073.

Zhao, X.J., Zhao, P.S., Xu, J., Meng, W., Pu, W.W., Dong, F., He, D., Shi, Q.F., 2013. Analysis of a winter regional haze event and its formation mechanism in the North China Plain. Atmos. Chem. Phys. 13, 5685-5696.

Zheng, G.J., Duan, F.K., Su, H., Ma, Y.L., Cheng, Y., Zheng, B., Zhang, Q., Huang, T., Kimoto, T., Chang, D., Pöschl, U., Cheng, Y.F., He, K.B., 2015. Exploring the severe winter haze in Beijing: the impact of synoptic weather, regional transport and heterogeneous reactions. Atmos. Chem. Phys. 15, 2969-2983.

Zheng, N., Liu, J., Wang, Q., Liang, Z., 2010. Health risk assessment of heavy metal exposure to street dust in the zinc smelting district, Northeast of China. Sci. Total Environ. 408, 726-733.

Figure Captions

Figure 1. Moderate resolution imaging spectroradiometer (MODIS) image (https://worldview.earthdata.nasa.gov/) showing a thick haze layer over the Northeast China plain and the transport paths over Northeast Asia influenced by the northwesterly wind, and a topographic map of Northeast China in the upper right corner. Air mass trajectories during the sampling period are shown in Figure S1.

Figure 2. Variations in the mass concentrations of $PM_{2.5}$, organic matter (OM), elemental carbon (EC), and water-soluble ions (Ca^{2+}, Mg^{2+}, K^{+}, NH_4^{+}, Na^{+}, SO_4^{2-}, NO_3^{-}, and Cl^{-}) from 28 January to 7 February 2015. The pink dates are the haze days.

Figure 3. Typical transmission electron microscopy (TEM) images and energy-dispersive X-ray spectrometry (EDS) spectra of different types of individual aerosol components: **(a)** dome-like organic particle, **(b)** irregular organic particle, **(c)** spherical organic particle, **(d)** soot particle coated by secondary organic aerosols (SOAs), **(e)** S-rich particle containing minor K and Si, and **(f)** fly ash particles.

Figure 4. Typical TEM images of individual internally mixed particles: **(a)** mixture of dome-like organic particle and S-rich particle (K); **(b)** mixture of irregular organic particle and S-rich particle (K) coated by SOAs; **(c)** mixture of spherical organic particle and S-rich particle (K) coated by SOAs; **(d)** mixture of irregular organic particle, soot, and S-rich particle (K); **(e)** mixture of S-rich particle (K), fly ash, and dome-like organic particle; and **(f)** mixture of S-rich particle (K) and metal particles (Pb) coated by SOAs.

Figure 5. Relative abundance of five types of individual particles from 28 January to 7 February 2015. A total of 1489 particles were analyzed, and the number of analyzed particles on each day is shown above the column.

Figure 6. Size distributions of individual particles on the non-haze (706 particles analyzed) and haze (783 particles) days. The distribution pattern is normalized.

Figure 7. Variations in SO_4^{2-}/EC, NO_3^{-}/EC, OC/EC, and $PM_{2.5}$/EC from 28 January to 7 February 2015.

Figure 8. Visibility photos and TEM images at low magnifications of individual aerosol particles on the non-haze and haze days: **(a)** aerosol particles on the non-haze days and **(b)** aerosol particles on the haze days.

588 **Figure 9.** Conceptual model (after Zheng et al. (2015)) of haze formation in winter in Northeast
589 China. The variations in $PM_{2.5}$/EC, NO_3^-/EC, OC/EC, and SO_4^{2-}/EC are from Figure 7, and the
590 variations in the meteorological conditions are from Figure S3. Emission sources were determined
591 from TEM observations of individual particles.


(Wind direction)
China
Lesser Khingan
Mountains
Sanjiang Plain
Harbin
Northeast
Plain
Changbai
Mountains
Changchun
Jilin
Shenyang
North Pacific
Bohai
Sea
Japan
Lesser Khingan Mountains
Harbin
Changchun
Jilin
Changbai Mountains
Shenyang

Figure 1.

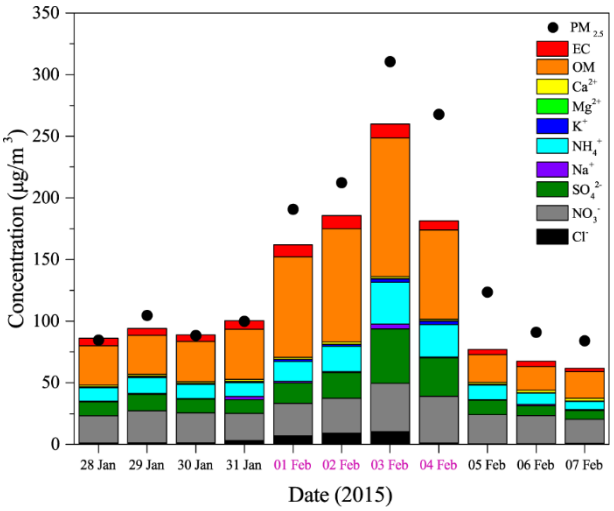
PM 2.5
EC
OM
Ca2+
Mg2+
K+
NH4+
Na+
SO42-
NO3-
Cl-
Concentration (μg/m3)
0
50
100
150
200
250
300
350
28 Jan
29 Jan
30 Jan
31 Jan
01 Feb
02 Feb
03 Feb
04 Feb
05 Feb
06 Feb
07 Feb
Date (2015)

Figure 2.

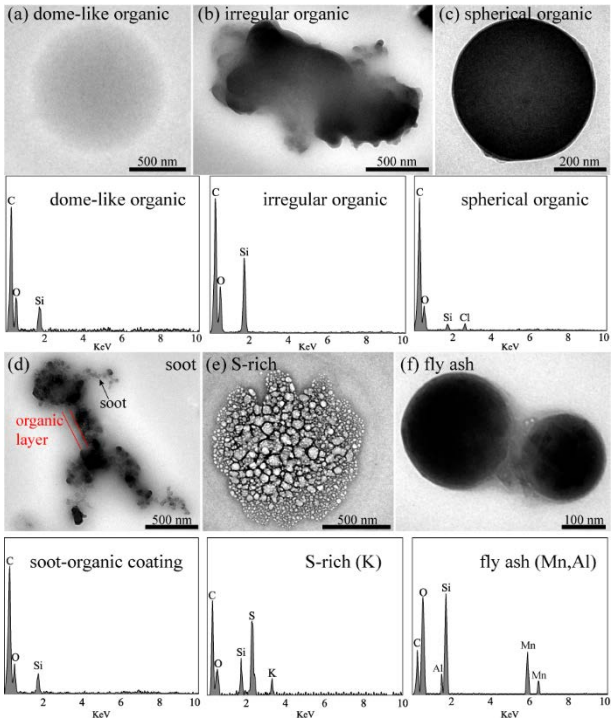

596

597 **Figure 3.**

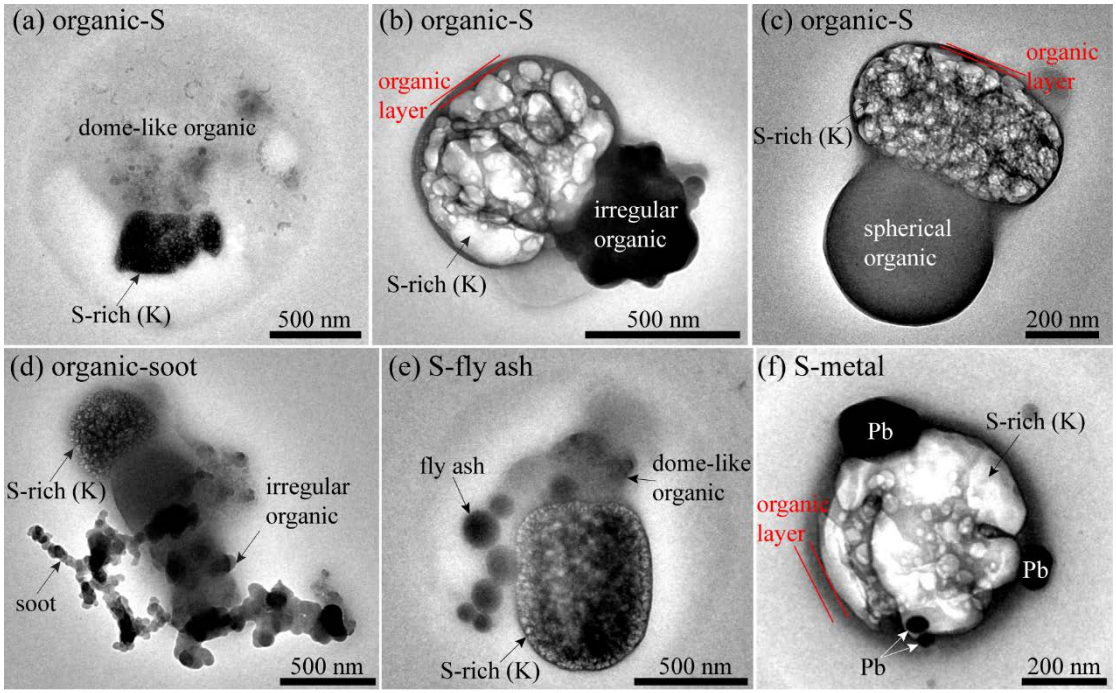
(a) organic-S
dome-like organic
S-rich (K)
500 nm
(b) organic-S
organic layer
irregular organic
S-rich (K)
500 nm
(c) organic-S
organic layer
S-rich (K)
spherical organic
200 nm
(d) organic-soot
S-rich (K)
irregular organic
soot
500 nm
(e) S-fly ash
fly ash
dome-like organic
S-rich (K)
500 nm
(f) S-metal
Pb
S-rich (K)
organic layer
Pb
Pb
200 nm

Figure 4.

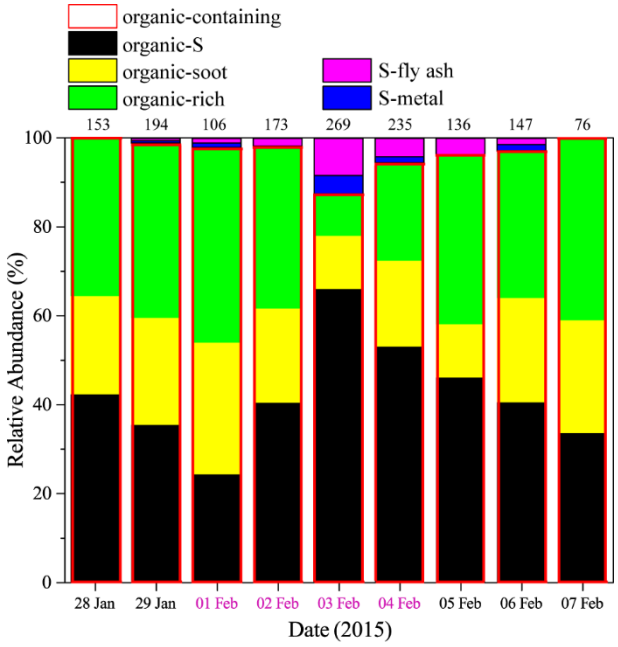

600

601 **Figure 5.**

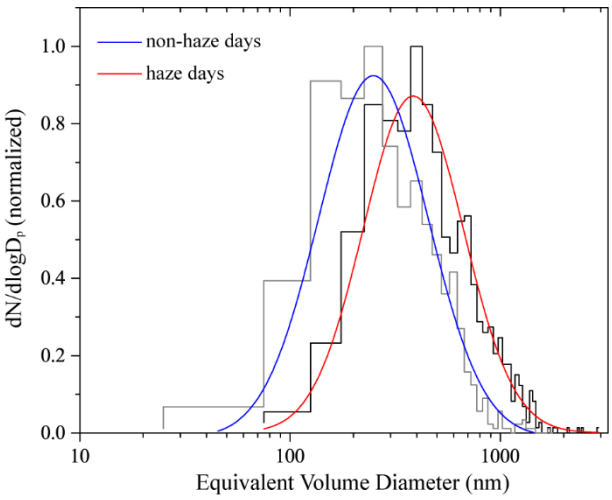

602

603 **Figure 6.**

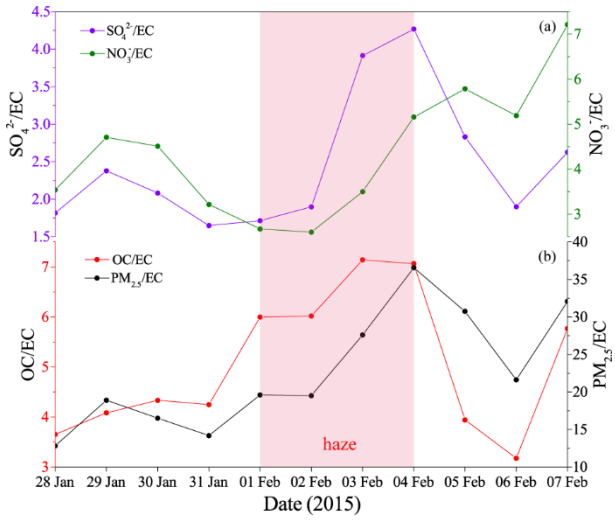

604

605 **Figure 7.**

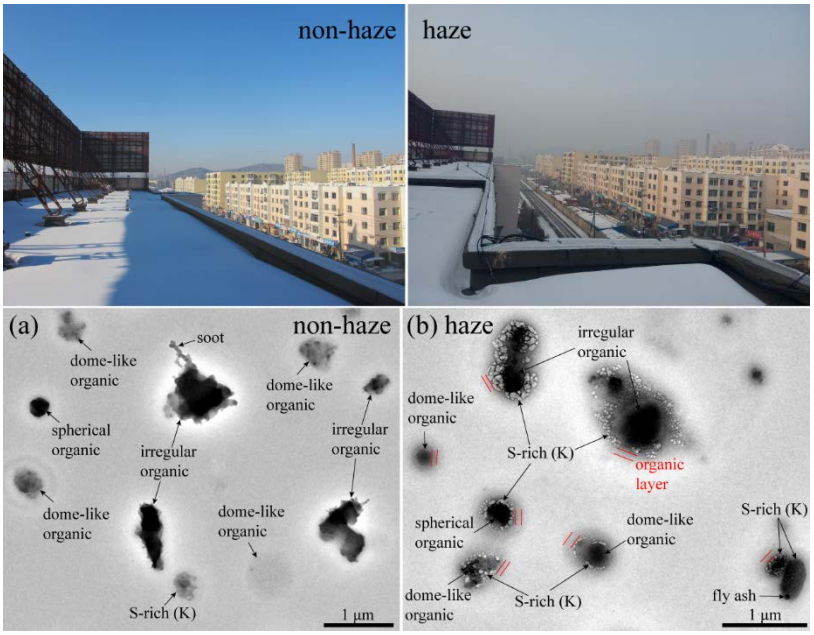

606

607 **Figure 8.**

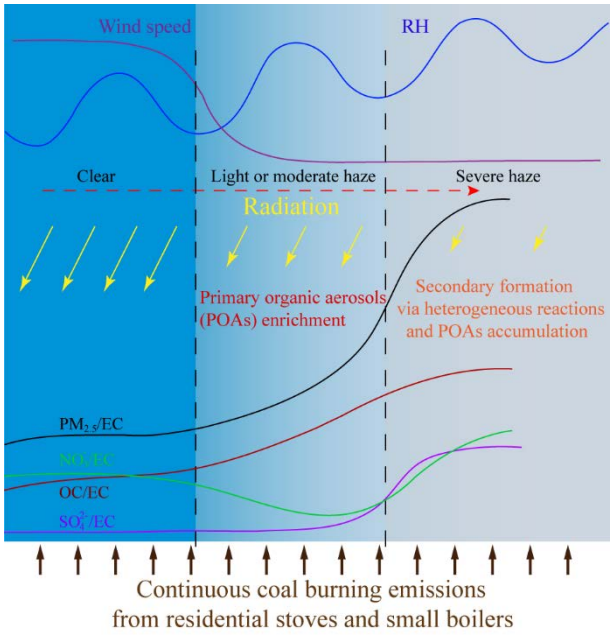

608

609 **Figure 9.**